Check for updates

Journal of Field Robotics

WILEY

RESEARCH ARTICLE

A Novel Multinozzle Targeting Pollination Robot for Clustered Kiwifruit Flowers Based on Air–Liquid Dual-Flow Spraying

Changqing Gao[1] | Leilei He[1] | Yusong Ding[1] | Bryan Gilbert Murengami[1] | Jinyong Chen[2,3] | Chengquan Zhou[4,5] | Hongbao Ye[4,5] | Rui Li[1] | Longsheng Fu[1]

[1]College of Mechanical and Electronic Engineering, Northwest A&F University, Yangling, Shaanxi, China | [2]Zhengzhou Fruit Research Institute, Chinese Academy of Agricultural Sciences, Zhengzhou, Henan, China | [3]National Key Laboratory for Germplasm Innovation & Utilization of Horticultural Crops, Zhengzhou, Henan, China | [4]Key Laboratory of Agricultural Equipment for Hilly and Mountainous Areas in Southeastern China (Co-construction by Ministry and Province), Ministry of Agriculture and Rural Affairs, Hangzhou, Zhejiang, China | [5]Institute of Agricultural Equipment, Zhejiang Academy of Agricultural Sciences, Hangzhou, China

Correspondence: Hongbao Ye (yhb2008@zaas.ac.cn) | Rui Li (ruili1216@nwafu.edu.cn) | Longsheng Fu (fulsh@nwafu.edu.cn)

Received: 9 June 2024 | **Revised:** 9 October 2024 | **Accepted:** 24 November 2024

Funding: This work was partially supported by the National Natural Science Foundation of China (No. 32371999), Science and Technology Program of Xi'an City, China (No. 23NYGG0071), National Key Research and Development Program of China (No. 2022YFD1600700), Open Project of Key Laboratory of Agricultural Equipment for Hilly and Mountainous Areas in Southeastern China (Co-construction by Ministry and Province), Ministry of Agriculture and Rural Affairs, China (No. QSKF2023002), Central Public-interest Scientific Institution Basal Research Fund (No. 1610192023105), and National Foreign Expert Project, Ministry of Science and Technology, China (Nos. DL2022172003L and QN2022172006L).

Keywords: clustered kiwifruit flowers | multinozzle end-effector-optimal | pollination robot | spray parameters

ABSTRACT

Manual pollination of kiwifruit flowers is a labor-intensive work that is highly desired to be replaced by robotic operations. In this research, a pollination robot was developed to achieve precision pollination of clustered kiwifruit flowers in the orchard. The pollination robot consists of five systems, including a multinozzle end-effector, a mechanical arm, a vision system, a crawler-type chassis, and a control system. The robot can select preferential flowers and then target their pistil to achieve precision pollination. First, statistical analysis of the dimensions of flower clusters and individual flowers was conducted to fit normal distribution curves, which guided the design of the spray coverage and combination intervals for the multinozzle end-effector. Second, optimal spray parameters were determined based on a three-factor, five-level quadratic orthogonal experiment, that is, air pressure of 70.4 kPa, rate of flow of 86.0 mL/min, and spray distance of 27.8 cm. A targeted pollination strategy was developed based on the preferential flower selection strategy and structure of the multinozzle end-effector. Field experiments were conducted in a commercial kiwifruit orchard to evaluate its feasibility and performance, and an average success targeting rate of 93.4% at an average speed of 1.0 s per flower was achieved. Furthermore, compared with artificial assisted pollination methods, it can improve the utilization rate of kiwifruit pollen with an average consumption of 0.20 g in every 60 flowers with an average fruit set rate of 88.9%. The validations demonstrated that the pollination robot can efficiently pollinate kiwifruit flowers and save pollen.

© 2025 Wiley Periodicals LLC.

1 | Introduction

Pollination plays a pivotal role in the production of kiwifruit, which significantly impacts kiwifruit yield and quality. Kiwifruit size is closely related to seed number, which depends on pollination (González, Coque, and Herrero 1995; Gheshlaghi 2019). Kiwifruit is dioecious and can only grow unisexual flowers, which requires cross-pollination (Jerram 1979; J. Li, Broussard, et al. 2022). Natural pollination alone cannot ensure sufficient pollination because of the staggered blooming periods of male and female flowers, as well as the lack of nectar in the flowers, making them less attractive to insects (Mcpherson et al. 2001; Castro et al. 2021). Kiwifruit flowers can be divided into multiple classes based on their phenology to select suitable flowers for pollination (Salinero, Vela, and Sainz 2009; Gianni and Vania 2018; G. Li, Fu, et al. 2022). Therefore, kiwifruit cultivation highly depends on assisted pollination.

Assisted pollination methods include artificial pollination and mechanized pollination. Artificial pollination is a labor-intensive process resulting in high labor costs and time-consuming (Johnson and Mooney 2014; Broussard et al. 2021; G. Li, Suo, et al. 2022). To address these challenges, numerous supplementary pollination approaches have emerged, several of which are adaptable to mechanized pollination. Tacconi et al. (2016) compared three mechanized pollination methods, including blower dry distributor of pure pollen, liquid distributor tractor machine, and a model utilizing tractor fans, all of which were verified to waste extra pollen. Wu et al. (2022) introduced a mobile kiwifruit atomizing sprayer for large-scale mechanized pollination, which consumed pollen at approximately 900 g/hm^2. Artificial and mechanized pollination still face issues of high labor intensity and pollen wastage, respectively. In addition, mechanical quantitative pollination remains a challenge.

Air–liquid dual-flow spraying could achieve quantified pollination and enhance pollen deposition. The air–liquid dual-flow pollination approach could fulfill quantified pollination by controlling the spraying time of prepared pollen liquid, which provides an easier medium for the rapid delivery of controlled polled doses (Williams et al. 2021). Since it does not directly contact stigma, it has the potential to enhance pollen utilization and heightened precision; thus, it exhibits substantial promise for kiwifruit robotic pollination (Hao et al. 2023). Gao et al. (2023) developed a pollination robot for preferential kiwifruit flowers based on a precise target with an air–liquid nozzle, which consumed 2.5×10^{-3} g pollen with a speed of 2.0 s for a single flower. However, prolonged pollen storage in liquid reduces its viability for large-scale field operations since the pollen absorbs water and begins to deteriorate after 2 h of immersion (Song et al. 2019; Chen, Wang, and Cheng 2021; Lippi et al. 2023). Thus, conducting research on air–liquid spray pollination is necessary, while also requiring enhanced efficiency to ensure complete pollination before pollen is inactivated in liquid.

The multinozzle targeting approach could be promising to improve pollination efficiency for flower clusters while ensuring the high utilization rate of pollen. Kiwifruit flowers grow in clusters, with multiple individual blooms grouped closely together on the vine (McNeilage 1991; Watson and Gould 1993; K. Li et al. 2023). Williams et al. (2020) designed a spray manifold consisting of 20 air-assisted nozzles linearly spaced 25 mm apart, which improved efficiency but did not reduce labor requirements regarding flower and fruit thinning because they did not pollinate preferential flowers (G. Li, Suo, et al. 2022; Bhattarai, Zhang, and Karkee 2024). Therefore, multinozzle targeting pollination for preferential kiwifruit flowers is a significant approach.

In this study, a pollination robot based on air–liquid dual-flow spraying and multinozzle targeting was designed for clustered kiwifruit flowers. For this pollination robot, a multinozzle end-effector, a mechanical arm, a crawler-type chassis, and a control system were designed and adopted for achieving preferential flower selection and precise target pollination. A field experiment verified the feasibility of this pollination robot and provided its performance compared with common artificial assisted approaches.

2 | Materials and Methods

2.1 | Composition of the Pollination Robot

The kiwifruit pollination robot encompassed five primary systems, facilitating the identification of appropriate flowers and subsequent precision targeting of flower clusters to achieve effective pollination. A three-dimensional structure of this robot is shown in Figure 1, which adopts a modular design and includes a multinozzle end-effector, a mechanical arm, a vision system, a crawler-type chassis, and a control system. The vision system incorporates an Red, Green, and Blue-Depth camera (RealSense D435, Intel, USA) for acquiring images of the kiwifruit canopy (Liu et al. 2024), with image processing techniques employed for detecting and localizing preferential flowers.

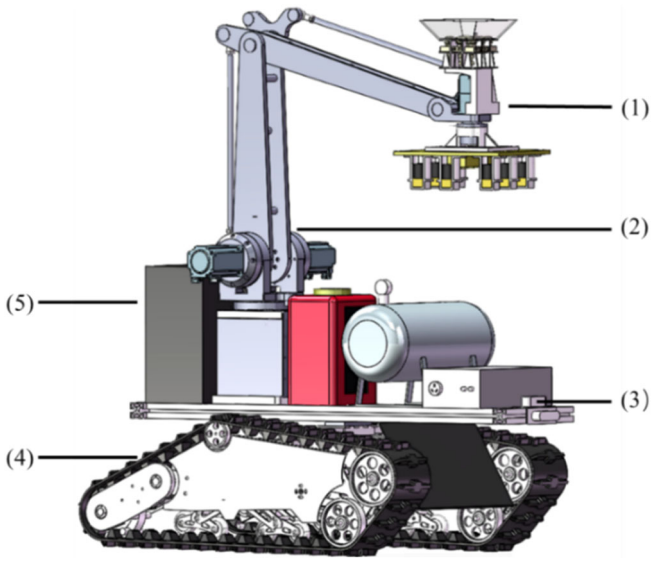


FIGURE 1 | Structure of kiwifruit pollination robot. (1) Multinozzle end-effector, (2) mechanical arm, (3) vision system, (4) crawler-type chassis, and (5) control unit.

15564967, 2025, 5, Downloaded from https://onlinelibrary.wiley.com/doi/10.1002/rob.22499 by Northwest Agri & Forestry, Wiley Online Library on [28/01/2026]. See the Terms and Conditions (https://onlinelibrary.wiley.com/terms-and-conditions) on Wiley Online Library for rules of use; OA articles are governed by the applicable Creative Commons License

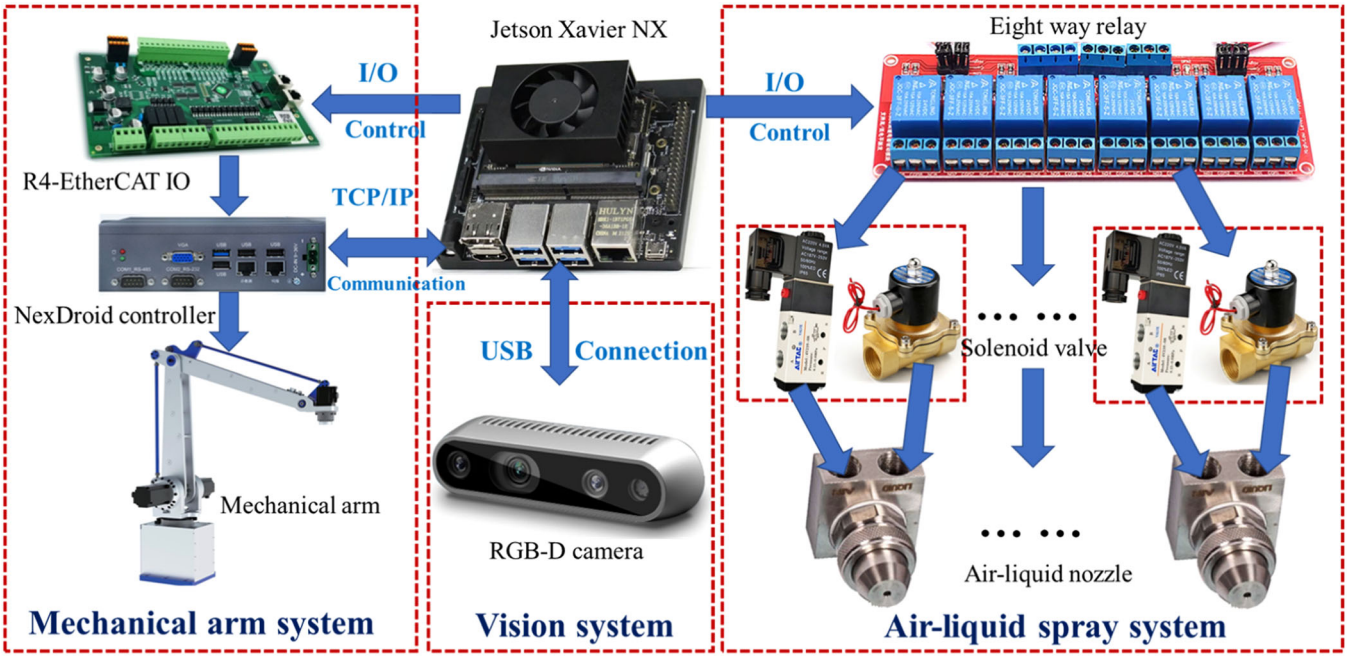


FIGURE 2 | The designed control system block diagram. I/O, input/output; RGB-D, Red, Green, Blue-Depth; TCP/IP, Transmission Control Protocol/Internet Protocol; USB, Universal Serial Bus.

The control system carries out information communication with the robotic arm, vision system, and air–liquid spray system through Transmission Control Protocol/Internet Protocol, USB interface, and serial bus, respectively. Figure 2 shows the overall structure of the control system. The main controller utilized for the control system is a Jetson Xavier NX module (NVIDIA, USA). First, the vision system detects and selects preferential flowers for pollination after acquiring canopy images. Then the vision system locates the target flowers based on the multinozzle target strategy. Three-dimensional coordinates of selected flowers are sent to the control system, which are transformed into coordinates of a mechanical arm. Finally, the robotic arm drives the end-effector with a spray system to pollinate clustered flowers based on multinozzle targeting strategies. After pollination of the current area is completed, the crawler-type chassis will move to the subsequent pollination zone.



FIGURE 3 | Example of the clustered growth characteristics for kiwifruit flowers.

2.2 | Multinozzle End-Effector Design

2.2.1 | Measurement and Analysis of Kiwifruit Flowers Size

The size of kiwifruit flowers was measured and analyzed for the multinozzle end-effector design. The growth characteristic of kiwifruit flowers is clustered, which is suitable for targeting pollination with multinozzles end-effector. An example of the growth and distribution of kiwifruit flowers in the canopy is shown Figure 3, where the yellow rectangles refer to kiwifruit flower clusters. In this research, the multinozzle end-effector and the corresponding pollination parameters were developed and designed to suit the shape and size of the kiwifruit flower clusters.

Sizes of 1255 kiwifruit flowers and 279 flower clusters were measured manually by vernier caliper and tape, which were analyzed to design end-effector. The collection of kiwifruit flower data was carried out at International Kiwifruit Innovation Orchard, Yangling, Shaanxi Province, China (34°17′ N, 108°2′ E, approximately 504 m in altitude). The diameter of the flower cluster is defined as the diagonal length of the minimum bounding rectangle. The average diameter of kiwifruit flower clusters (ad_{fc}) was 26.5 cm, with a standard deviation $\sigma_{fc} = 10.9$ cm, as shown in Figure 4a. Therefore, the overall spray coverage of the multinozzle end-effector should encompass ad_{fc}. Besides, the average diameter of kiwifruit flowers (ad_f) was 55.3 mm, with a standard deviation $\sigma_f = 9.8$ mm, as illustrated in Figure 4b. The measured average diameter of the pistil area (ad_p) was 24.3 mm, with a standard deviation $\sigma_p = 12.4$ mm, as shown in Figure 4c. Thus, to economize pollen while ensuring pollination efficiency, the spray coverage should be between ad_f and ad_p.

15564967, 2025, 5, Downloaded from https://onlinelibrary.wiley.com/doi/10.1002/rob.22499 by Northwest Agri & Forestry, Wiley Online Library on [28/01/2026]. See the Terms and Conditions (https://onlinelibrary.wiley.com/terms-and-conditions) on Wiley Online Library for rules of use; OA articles are governed by the applicable Creative Commons License

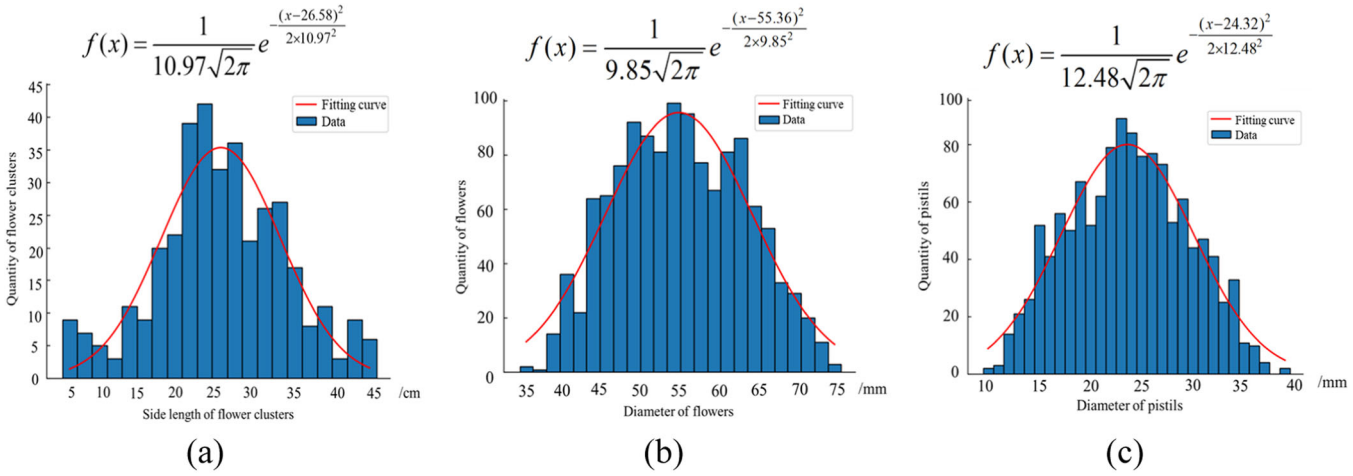


FIGURE 4 | Distribution of kiwifruit flowers dimension measurements. (a) Minimum bounding rectangle side length of kiwifruit flower clusters, (b) external circle diameter of kiwifruit flowers, and (c) external circle diameter of the pistil area of kiwifruit flowers.

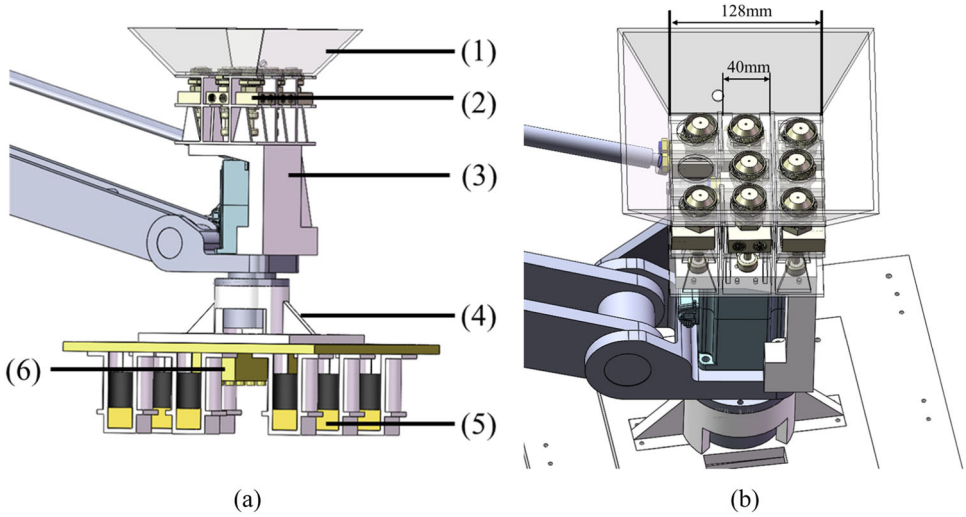


FIGURE 5 | Construction of the multinozzle end-effector, including pollen liquid recovery device (1), air–liquid nozzle (2), nozzles mounting bracket (3), solenoid valves mounting bracket (4), liquid solenoid valves (5), and air solenoid valves (6). Its front view (a) and oblique view (b) are also displayed.

2.2.2 | Multinozzle End-Effector Design

The multinozzle end-effector was designed based on the size of flower clusters and distribution of flowers to achieve targeted pollination while enhancing efficiency. The end-effector consisted of eight air–liquid dual-flow channels, a pollen liquid recovery device, and mounting brackets, as shown in Figure 5a. Specifically, an air–liquid dual-flow channel includes an air–liquid nozzle, a liquid solenoid valve, and a solenoid valve. And eight air–liquid nozzles are uniformly arranged in a 3×3 matrix with a side length of 128 mm, as illustrated in Figure 5b. Among them, the side length of a single nozzle is 40 mm, with a 2-mm spacing between each nozzle.

The dual-flow unit is the crucial component in the multinozzle end-effector, which affects the spraying and pollination effects. It consists of a dual-flow nozzle, an air pump, an electric fluid tank, and measurement devices, as shown in Figure 6. Specifically, an air pump (750 W–30 L, Outstanding, China) and an electric pollen fluid tank (6 L, KeNeng, China) were adopted to provide power for air path and liquid path, respectively. Two throttle valves (SA-8, ZhuoJi, China) were employed to regulate the flow of air path and liquid path, and their corresponding air pressure and rate of flow were measured by a pressure transmitter (HC-P30, Hosswill, China) and a float flowmeter (DFG-6 T, Darhor, America). For this spray system, a 1-mm aperture conical dual-flow nozzle (JAC, ShaOu, China) was utilized, with the air pressure and liquid flow adjusted to produce an appropriate droplet size of the prepared pollen liquid for kiwifruit flower pollination. In addition, relays control the response time of both the air solenoid valve (VT307, SMC, Japan) and liquid solenoid valve (N2W, CHNT, China), thereby regulating spray coverage and quantity of pollen for achieving precise pollination, respectively.

15564967, 2025, 5, Downloaded from https://onlinelibrary.wiley.com/doi/10.1002/rob.22499 by Northwest Agri & Forestry, Wiley Online Library on [28/01/2026]. See the Terms and Conditions (https://onlinelibrary.wiley.com/terms-and-conditions) on Wiley Online Library for rules of use; OA articles are governed by the applicable Creative Commons License

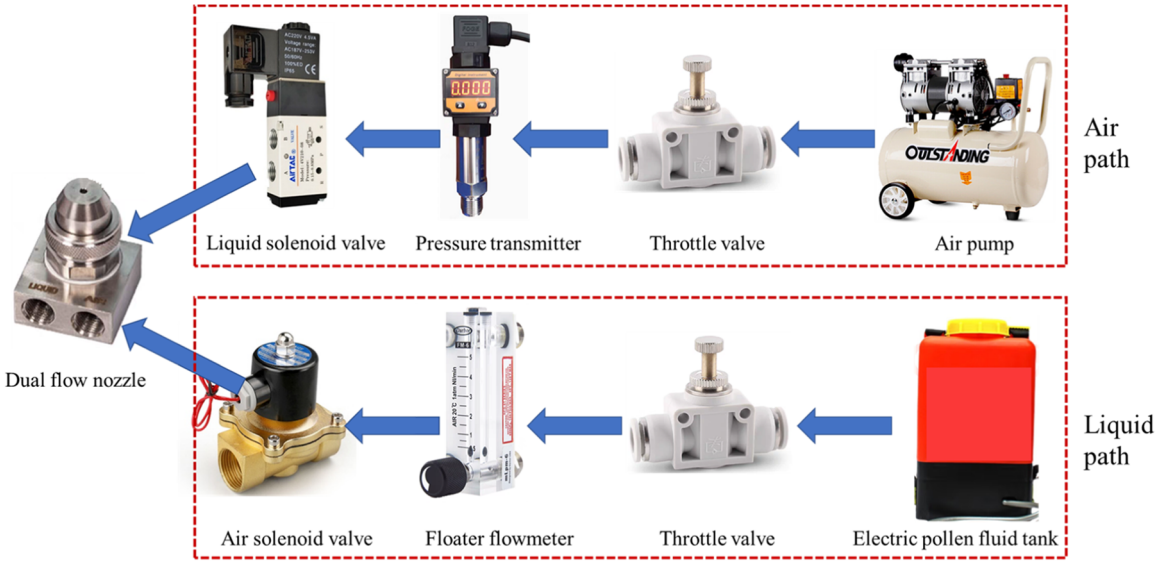


FIGURE 6 | Composition of dual-flow unit.

2.3 | Optimal Spray Parameters

Pollination effectiveness is significantly impacted by the spray parameters, which are responsible for controlling the spray volume of the pollen suspension. The performance of multinozzle targeting pollination with parameter combinations was assessed by pollen fluid deposition and fraction of coverage, where pollen fluid deposition represents how much pollen could attach to flower, and fraction of coverage indicates the area of pollen deposited in the pistil region (Meshram et al. 2022; Lohan et al. 2022). The rate of flow affects the deposition amount, while spray distance and air pressure both affect the spray coverage and deposition. The experimental factors selected are air pressure (X_1), rate of flow (X_2), and spray distance (X_3). The evaluation criteria include pollen fluid deposition (Y_1) and fraction of coverage (Y_2). Combining theoretical analysis with the results of single-factor experiments, experimental factor codes were set, as shown in Table 1. The experiment was arranged utilizing a three-factor, five-level quadrature rotation combination design, and each experimental combination was repeated three times.

TABLE 1 | Level of the test factors for selecting optimal spray parameters.

	Factors		
Code	Air pressure (kPa)	Rate of flow (mL/min)	Spray distance (cm)
−1.682	30	50	10
−1	40	55	15
0	65	75	25
1	90	90	35
1.682	100	95	40

2.3.1 | Measurement of Pollen Liquid Deposition

The measurement platform for spray parameters selection is shown in Figure 7, which consists of a droplet collecting plate, spray distance measuring ruler, multinozzle end-effector, and distance adjustment angle iron. To better show the effect of the main variables on the results, the response surface model is simplified so that minor variables are ignored (Zhang et al. 2005; Reji and Kumar 2022). Therefore, the influence between adjacent nozzles was ignored in this study. When the spray parameters of each nozzle are set the same, the deposition amount and coverage of each nozzle are assumed to be the same. Therefore, the spray overlap area can be determined based on the spacing of each nozzle. Additionally, the overlap area is within the petal region, and measuring the pistil region will not be affected. Thus, this experiment is testing the optimal spray parameters for a single nozzle.

Pollen drops collection plate consists of an annular section with an inner diameter of 30 mm and an outer diameter of 60 mm, corresponding to the pistil and petal areas of kiwifruit flowers, respectively, as shown in Figure 8. Liquid composition in the spray test was similar to that in the pollination test, that is, 10% sucrose, 0.01% boric acid, 0.2% agar, 0.1% pollen, and water 89.69%. The plate was adopted for the measurement of pollen liquid deposition. During measurements, the collection plate was positioned 10–40 cm directly above the nozzle, aligning the center of the plate with the center of the spray orifice. After sampling, the collection plate was taken down, and the masses of the circular piece and the annular section were individually measured using an electronic balance with a precision of 0.1 mg (AL204 model, Mettler Instruments Limited). The mass difference of the collection plate before and after spraying represents the deposition mass of pollen droplets in the plate.

2.3.2 | Measurement of Spray Coverage

Droplet distribution was collected by water-sensitive paper (SixSix Mountain Plant Protection Technology Company) with a shape of $3 \times 11\ cm^2$. After the water-sensitive paper was air-

15564967, 2025, 5, Downloaded from https://onlinelibrary.wiley.com/doi/10.1002/rob.22499 by Northwest Agri & Forestry, Wiley Online Library on [28/01/2026]. See the Terms and Conditions (https://onlinelibrary.wiley.com/terms-and-conditions) on Wiley Online Library for rules of use; OA articles are governed by the applicable Creative Commons License

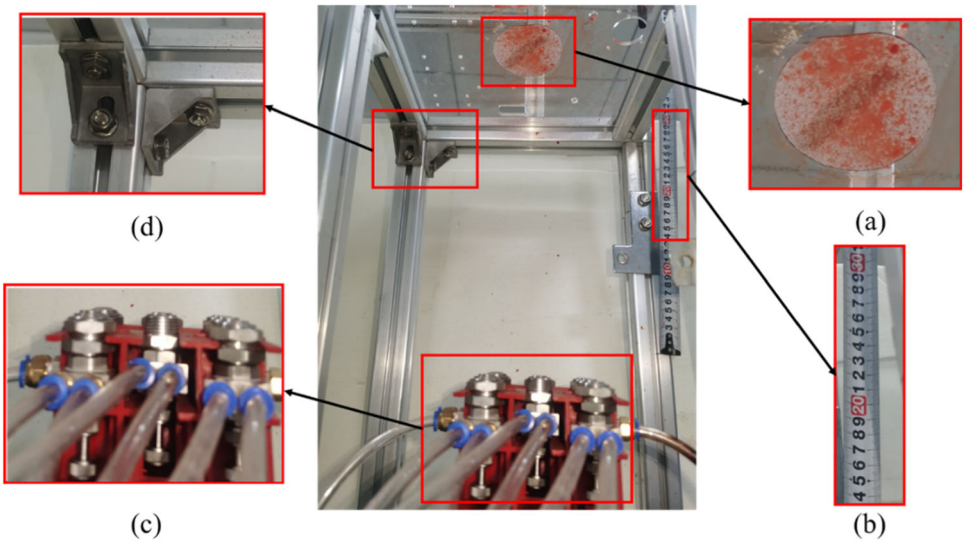


FIGURE 7 | Spray parameters selection measurement platform. (a) Droplet collecting plate, (b) spray distance measuring ruler, (c) multinozzle end-effector, and (d) distance adjustment angle iron.

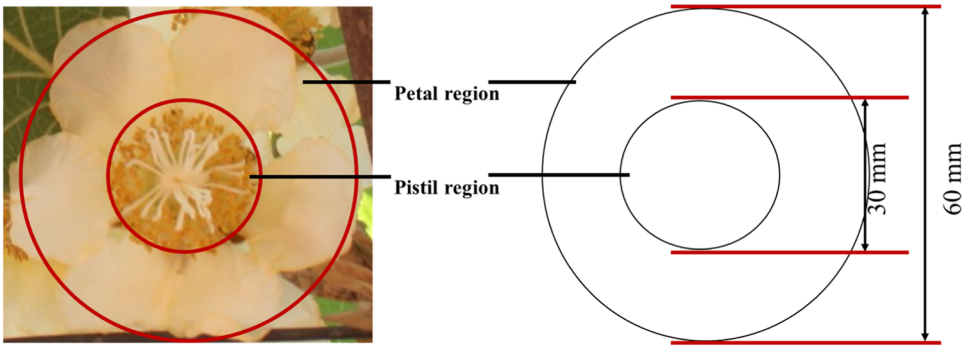


FIGURE 8 | Example of measurement of pollen liquid deposition. The middle area between the outer red circle and the inner red circle in the left image is the petal region, while the inner red circle represents the pistil region.

dried, a scanner (HP LaserJet MFPM 233dw) was employed to capture images of the droplet imprints on the water-sensitive paper. The area measurement function of ImageJ (National Institutes of Health) software was utilized to analyze the droplet coverage within each rectangular region obtained by sequentially cropping $3 \times 3\,cm^2$ areas from left to right on the water-sensitive paper image, as shown in Figure 9.

2.4 | Multinozzle Targeting Strategy

2.4.1 | Flower Detection and Selection

There are various flower phenological stages within canopy at the same, but only the flowers in certain stages are suitable for pollination (Gianni and Vania 2018). Original images were acquired at different natural lighting conditions to enhance the generalization ability of the detection model. Besides, a RealSense D435 camera with adaptive exposure was used to capture canopy images, which could reduce the impact of varying lighting conditions on flower detection to a certain extent. You Only Look Once (YOLO) model, demonstrated exceptional speed while maintaining high accuracy in agricultural applications (Fan et al. 2023; Gao et al. 2024; H. Li et al. 2024). Therefore, a multiclass detection method based on YOLOv8m was adopted to detect and determine the suitable phenological stages of kiwifruit flowers. After that, a selection approach was achieved by combining kiwifruit flower pollination agronomy with canopy flower distribution, which determined the preferential flowers for pollination. The detailed description of the specific execution of the method of flower selection utilized in this research has been expounded upon in the prior study by G. Li, Fu et al. (2022).

2.4.2 | Targeting Strategy

Multinozzle targeting strategy was developed based on spray coverage, distribution of Euclidean distances of flowers, and preferential flower selection strategy for pollination. First, preferential flowers are obtained based on the multiclass detection method and preferential flower selection strategy, as shown in Figure 10a. Next, determined spray coverage by experiment of optimal spray parameters selection is utilized to match nozzles with the flower clusters. Specifically, the closest pistil to the center point of the detected flower cluster rectangle is determined based on the Euclidean distance, as shown in Figure 10a.

15564967, 2025, 5, Downloaded from https://onlinelibrary.wiley.com/doi/10.1002/rob.22499 by Northwest Agri & Forestry, Wiley Online Library on [28/01/2026]. See the Terms and Conditions (https://onlinelibrary.wiley.com/terms-and-conditions) on Wiley Online Library for rules of use; OA articles are governed by the applicable Creative Commons License



FIGURE 9 | Analysis of water-sensitive paper for spray coverage. (a) Original water-sensitive paper, (b) scanned image of sprayed water-sensitive paper after drying, and (c) binarized scanned image for coverage analysis in ImageJ software.

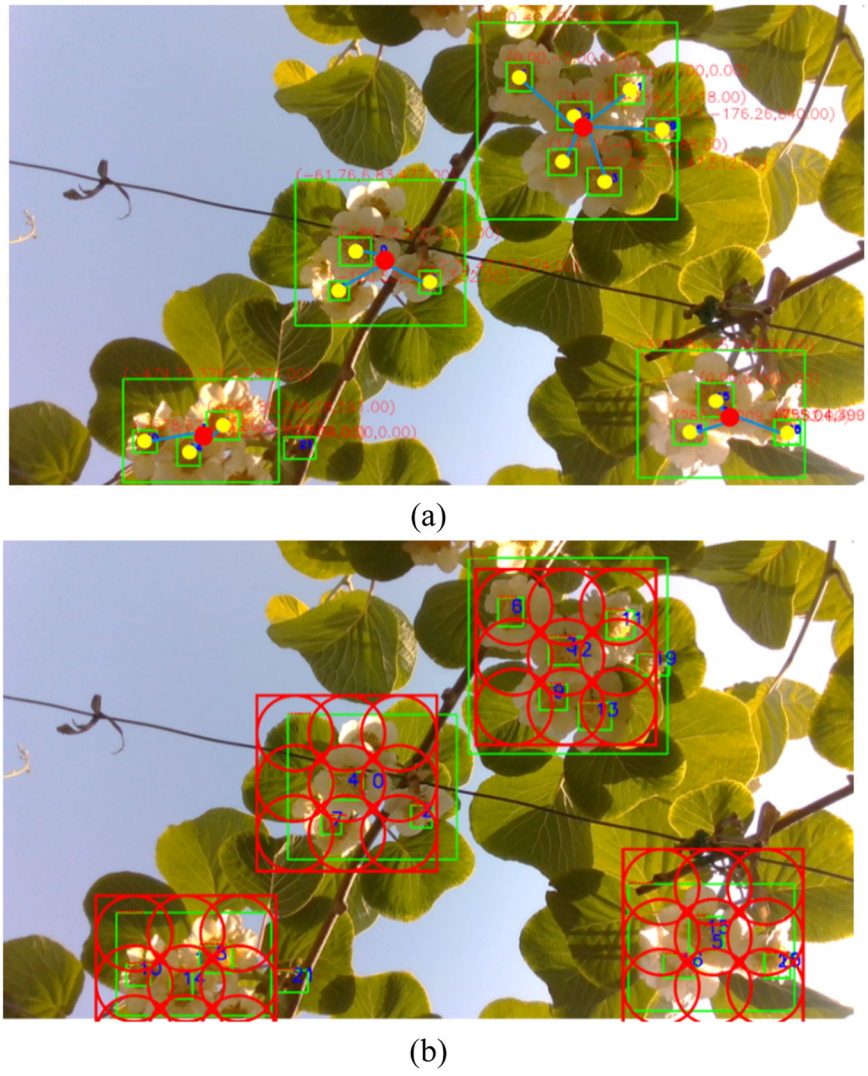


FIGURE 10 | Multinozzle targeting strategy diagram. (a) Selecting the nearest flower to the center of the flower cluster detection rectangle for the central nozzle to target based on Euclidean distance. Red points and yellow points represent the center of flower cluster detection rectangles and flower detection rectangles, respectively. (b) Spray coverage determines which nozzle activates. The red rectangle represents the external rectangle for spray coverage, and the circles inside the rectangle indicate the spray coverage of each nozzle.

Then the central nozzle of the multinozzle end-effector will target the determined pistil. Subsequently, if the spray coverage of the remaining nozzles can cover 80% of the corresponding region of pistils, the air solenoid valve and liquid solenoid valve will respond corresponding to the respective nozzle to achieve pollination (as depicted in Figure 10b). If the number of pollinated flowers meets the requirements (i.e., 3–5 flowers pollinated in a cluster), the operation proceeds to the next flower cluster. In cases where the requirements are not fulfilled, a secondary targeting action is

15564967, 2025, 5, Downloaded from https://onlinelibrary.wiley.com/doi/10.1002/rob.22499 by Northwest Agri & Forestry, Wiley Online Library on [28/01/2026]. See the Terms and Conditions (https://onlinelibrary.wiley.com/terms-and-conditions) on Wiley Online Library for rules of use; OA articles are governed by the applicable Creative Commons License

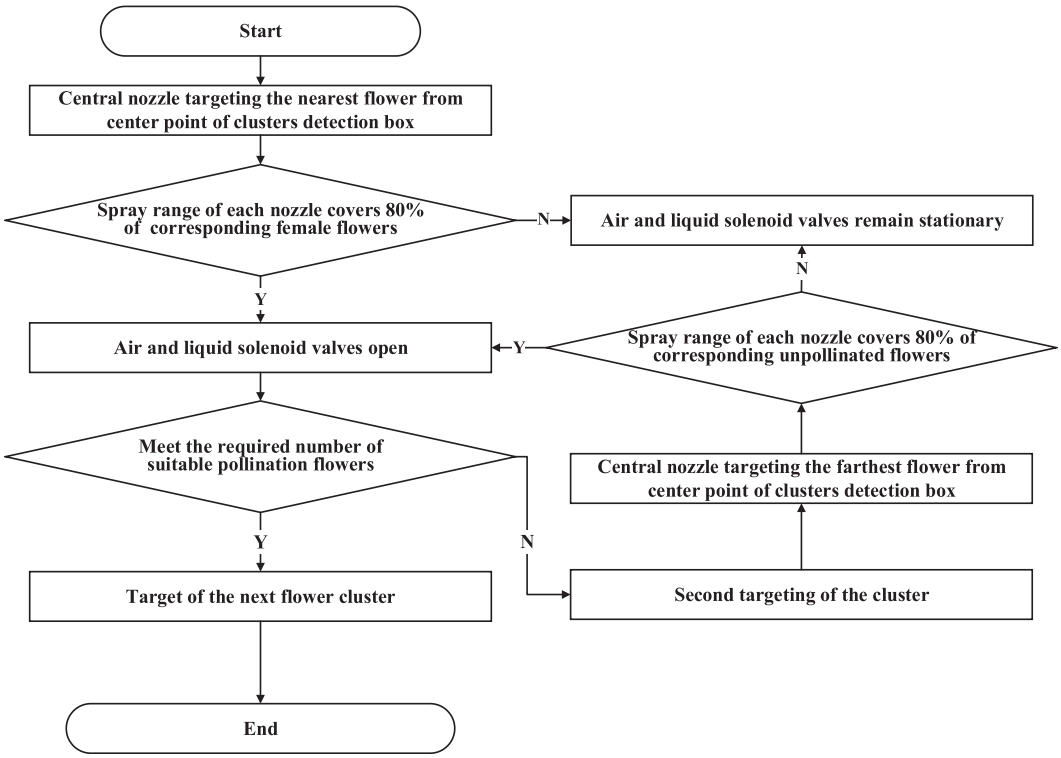


FIGURE 11 | Flowchart of multinozzle targeting strategy for kiwifruit pollination robot.

initiated. The flowchart of the targeting strategy is shown in Figure 11.

2.5 | Pollination Experiment in Orchard

The pollination robot was tested in International Kiwifruit Innovation Orchard, Yangling, Shaanxi Province, China (34°17′ N, 108°2′ E, approximately 504 m in altitude), and evaluated its feasibility, in May 2023. For this orchard, a standard trellis planting mode was adopted for kiwifruits, which can provide a simple and structured workspace for robotic pollination.

Kiwifruit orchard was evenly partitioned into five subregions according to its area to make the pollination experimental to be representative. And the pollination experimental zone was randomly selected in each subregion. Each designated zone centered around a single kiwifruit plant, serving as the subject for the pollination experiments, covering an area of $3 \times 3\,m^2$, a total of five areas. A total of 912 kiwifruit flowers in the experimental areas were pollinated based on a preferential flower selection strategy. Concurrently, diverse artificial assisted pollination techniques, specifically hand pollination and electric sprayer with liquid pollination, were employed across distinct zones within the orchard to assess the efficacy of the pollination robot.

For this pollination robot, a selective strategy based on multiclass kiwifruit flower detection and its distribution was applied to select preferential flowers for pollination. In addition, a multinozzle targeting strategy was adopted to target flowers in clusters. An example of kiwifruit pollination robot operation scene in field experiments is shown in Figure 12. Four months after pollination, fruits pollinated by robot were harvested. A total of 60 fruits pollinated by electric sprayer and hand pollination were harvested randomly for comparison, with their weights and quantities of seeds measured in each.

2.6 | Performance Evaluation

Evaluation metrics, that is, Average Precision (*AP*), mean Average Precision (*mAP*), and detection speed, were employed to assess trained multiclass flower detection models on the test data set. *AP* represents the area under the Precision-Recall curve (with Precision on the vertical axis and Recall on the horizontal axis) as shown in Equation (1), served as the measured ability of models to detect individual classes. Meanwhile, *mAP*, as defined in Equation (2), quantified the average *AP* across the 14 classes. And higher *AP* and *mAP* collectively indicated superior detection performance of the deep learning models for given objects.

$$AP = \int_0^1 P_{(R)}\, dR, \tag{1}$$

$$mAP = \frac{1}{k}\sum_{i=1}^{k} AP_i. \tag{2}$$

Consumption of pollen (P_c) by the robot can be estimated as illustrated in Equation (3). Specifically, C_p, V_s, and N_f represent concentration of pollen, volume of liquid per spray, and the number of shots fired for flowers, respectively. Success rate of targeting (S_t) is defined in Equation (4), which is measured as the number of hit flowers (F_h) over the total number of flowers that were selected by the vision system (F_s). The success rate of flower detection (S_{fd}) is described as the number of flowers

15564967, 2025, 5, Downloaded from https://onlinelibrary.wiley.com/doi/10.1002/rob.22499 by Northwest Agri & Forestry, Wiley Online Library on [28/01/2026]. See the Terms and Conditions (https://onlinelibrary.wiley.com/terms-and-conditions) on Wiley Online Library for rules of use; OA articles are governed by the applicable Creative Commons License

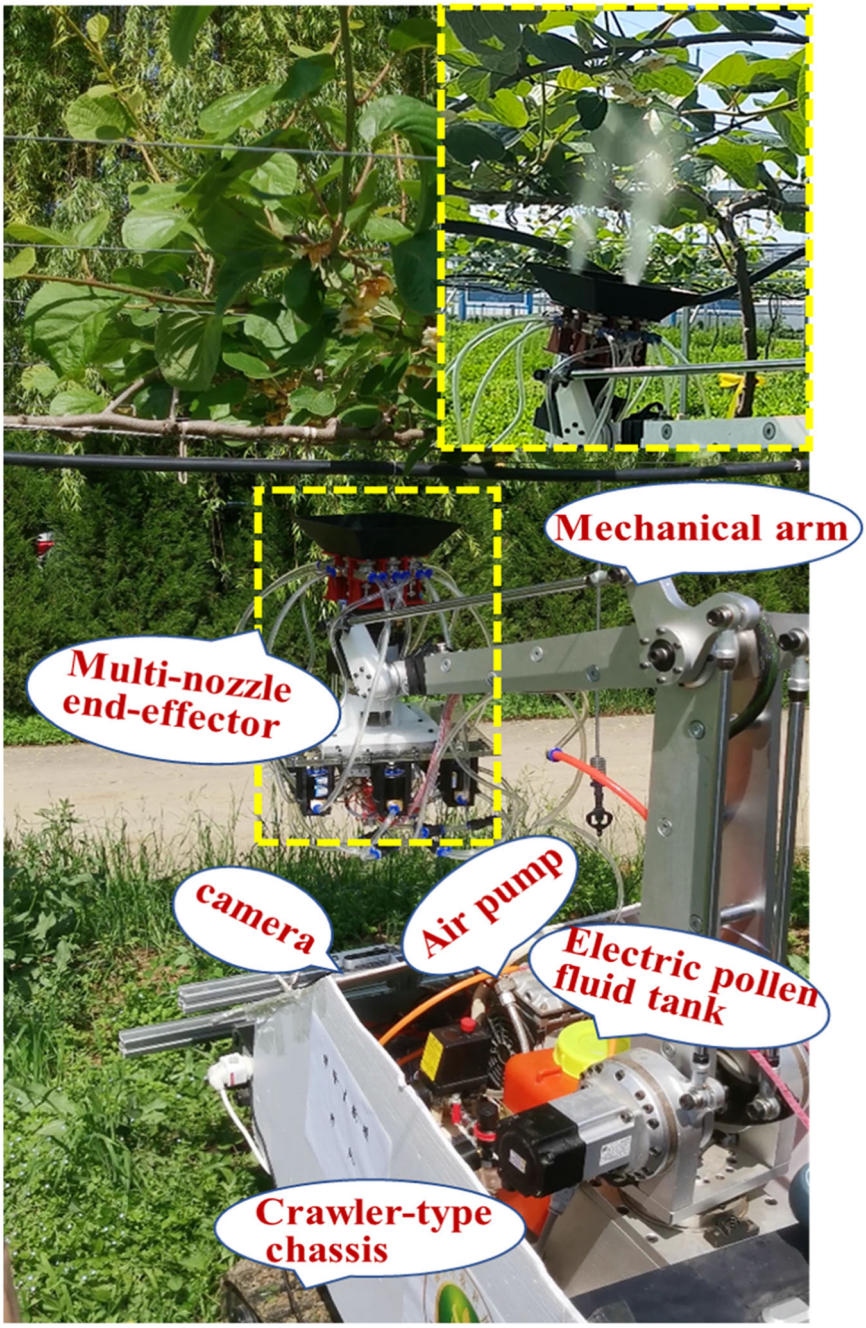


FIGURE 12 | Field experiment scene of kiwifruit pollination robot. Bubble diagrams describe the composition of the robot, and yellow rectangles show the operation scene of the multinozzle end-effector.

detected by model (D_m) after removing false detections (F_d) and missed flowers (M_f) divided by the total number of flowers (T_f) in the image, as shown in Equation (5). The fruit set rate (F_{sr}) is defined as the number of flowers that produce fruit (F_{pf}) divided by the number of pollinated flowers (P_f), as shown in Equation (6), where the F_{pf} is measured 20 days after pollination. Additionally, the detection speed of trained YOLOv8m and pollination speed of robot were computed as part of the evaluation process.

$$P_c = C_p \times V_s \times N_f, \tag{3}$$

$$S_t = \frac{F_h}{F_s}, \tag{4}$$

$$S_{fd} = \frac{D_m - F_d - M_f}{T_f}, \tag{5}$$

$$F_{sr} = \frac{F_{pf}}{P_f}. \tag{6}$$

3 | Results and Discussion

3.1 | Kiwifruit Flower Detection

Speed and accuracy of flower detection can meet the requirements of a multinozzle pollination robot. The *mAP* of 98.4% on multiclass flower detection was obtained by YOLOv8m. The average flower detection speed of YOLOv8m in an image with

15564967, 2025, 5, Downloaded from https://onlinelibrary.wiley.com/doi/10.1002/rob.22499 by Northwest Agri & Forestry, Wiley Online Library on [28/01/2026]. See the Terms and Conditions (https://onlinelibrary.wiley.com/terms-and-conditions) on Wiley Online Library for rules of use; OA articles are governed by the applicable Creative Commons License

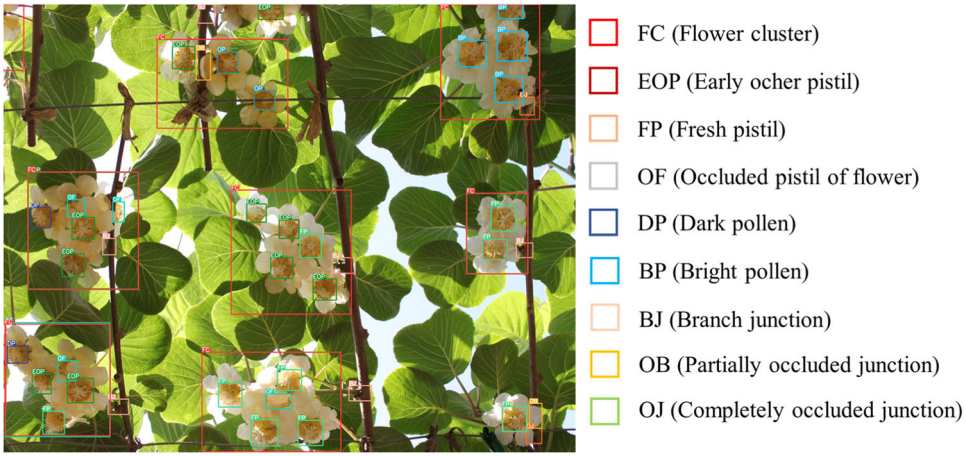


FIGURE 13 | Examples of multiclass flower and flower clusters detected by YOLOv8m. YOLO, You Only Look Once.

1280 × 720 pixels was 13.3 ms, which can meet the requirement for real-time kiwifruit flower pollination. The flower detection success rate was 98.9% in the field pollination experiment. An example of multiclass flower detection is shown in Figure 13.

3.2 | Optimal Spray Parameters

3.2.1 | Regression Model

A regression model for the optimal spray parameters was established based on a three-factor, five-level orthogonal rotation combination experiment. According to experimental results in Section 2.3, utilizing pollen fluid deposition (Y_1) and a fraction of coverage (Y_2) as response variables, the factors under consideration include air pressure (X_1), rate of flow (X_2), and spray distance (X_3). Incorporating the sum of squares and degrees of freedom of nonsignificant interaction terms into residual terms, the regression equations for the impact of various factors on Y_1 and Y_2 are obtained through analysis of variance, as shown in Equations (7) and (8). Multiple correlation coefficients (R^2) of the predictive model were 0.91 and 0.86, indicating its high reliability.

$$\begin{aligned} Y_1 = &-0.38 + 1.06 \times 10^{-3}X_1 + 1.37 \times 10^{-2}X_2 \\ &+ 2.50 \times 10^{-3}X_3 \\ &+ 4.00 \times 10^{-5}X_1X_2 - 1.00 \times 10^{-4}X_2X_3 \\ &- 3.70 \times 10^{-5}X_1^2 - 7.50 \times 10^{-5}X_2^2, \end{aligned} \tag{7}$$

$$\begin{aligned} Y_2 = &-95.79 + 1.78X_1 + 0.89X_2 + 5.42X_3 \\ &+ 2.50 \times 10^{-2}X_1X_3 \\ &- 3.00 \times 10^{-2}X_2X_3 - 1.55 \times 10^{-2}X_1^2 \\ &- 8.68 \times 10^{-2}X_3^2. \end{aligned} \tag{8}$$

3.2.2 | Response Surface Analysis

Within the range of experimental parameters, pollen fluid deposition first increases and then decreases with the increase in rate of flow, and decreases with the increase in air pressure. Figure 14a illustrates the effect of air pressure and flow rate on pollen fluid deposition at a spray distance of 25 cm. It can be observed that when the air pressure increases from 40 to 90 kPa, the pollen fluid deposition first increases to approximately 0.22 g and then decreases to nearly 0.08 g. When the rate of flow increases from 55 to 90 mL/min, the pollen fluid deposition increases first and then decreases, but the change is not significant

Within the range of experimental parameters, the pollen fluid deposition gradually increases with the increase of liquid flow rate and the decrease of spray distance. Figure 14b shows the effect of spray distance and flow rate on pollen fluid deposition at a constant air pressure of 65 kPa. The results indicate that when the spray distance increases from 15 to 35 cm and the flow rate increases from 55 to 90 mL/min, the pollen fluid deposition increases from approximately 0.08 g to over 0.25 g. Notably, under a shorter spray distance of 15 cm and a higher flow rate of 90 mL/min, the pollen fluid deposition reaches its maximum.

The fraction of coverage increases with the rise in air pressure and spray distance and varies with changes in rate of flow. Figure 15a illustrates the effect of air pressure and spray distance on the fraction of coverage at 72.5 mL/min rate of flow. As air pressure increases from 40 to 90 kPa, the fraction of coverage first increases and then decreases. And as spray distance increases from 15 to 35 cm, the fraction of coverage has a similar change pattern. Specifically, the entire response surface forms an arch shape with a maximum value. The highest coverage is achieved under high air pressure (around 80 kPa) and moderate spray distance (around 25 cm). Figure 15b shows the effect of spray distance and flow rate on the fraction of coverage at a constant air pressure of 65.0 kPa. The results indicate that when the spray distance increases from 15 to 35 cm, the fraction of coverage first increases to 80% and then decreases to 70%. As the rate of flow increases from 55 to 90 mL/min, it increases from approximately 55% to 60%. Particularly, under moderate spray distance (around 25 cm) and higher flow rate (around 90 mL/min) conditions, the fraction of coverage reaches its maximum. This indicates that within a certain range, increasing air pressure with

15564967, 2025, 5, Downloaded from https://onlinelibrary.wiley.com/doi/10.1002/rob.22499 by Northwest Agri & Forestry, Wiley Online Library on [28/01/2026]. See the Terms and Conditions (https://onlinelibrary.wiley.com/terms-and-conditions) on Wiley Online Library for rules of use; OA articles are governed by the applicable Creative Commons License

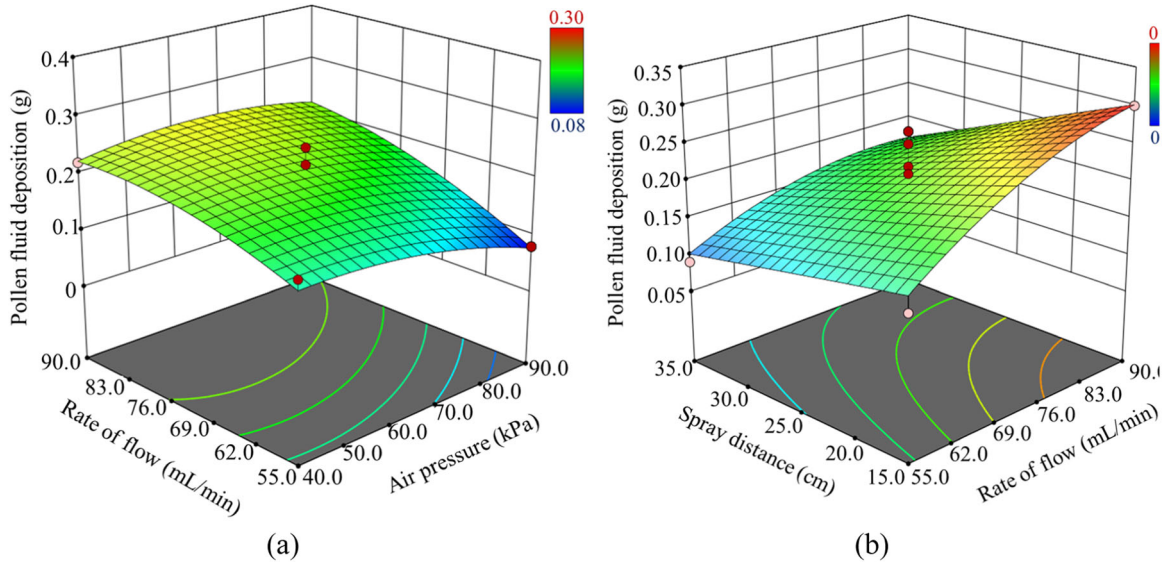


FIGURE 14 | Response surface of pollen fluid deposition. (a) Pollen fluid deposition with constant spray distance and (b) pollen fluid deposition with constant air pressure. The color scale goes from pollen fluid deposition of 0.08 g, represented in blue, through yellow, and finally to 0.30 g, in red.

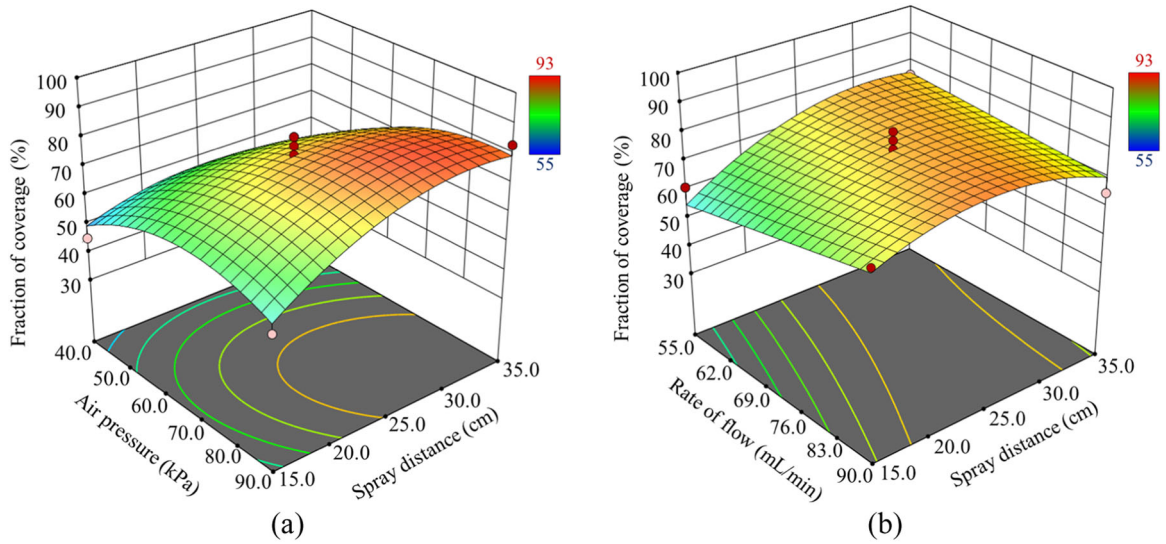


FIGURE 15 | Response surface of a fraction of coverage. (a) Fraction of coverage with a constant rate of flow and (b) fraction of coverage with constant air pressure. The color scale goes from pollen fluid deposition of 55%, represented in blue, through yellow, and finally to 93%, in red.

adjusting spray distance and rate of flow can improve the fraction of coverage.

Spray distance, air pressure, and rate of flow are crucial factors affecting pollen deposition, and optimizing these parameters could enhance pollen fluid deposition. A multi-objective optimization algorithm resulted in the refinement of optimal parameters, with an air pressure of 70.4 kPa, a rate of flow of 86.0 mL/min, and a spray distance of 27.8 cm. Pollen fluid deposition and fraction of coverage determined by the parameters are 90.1% and 0.21 g, respectively, which directly impact targeting efficiency and accuracy of multiple nozzles, thereby influencing fruit setting rate and kiwifruit quality.

3.3 | Performance Validation of the Developed Pollination Robot

Evaluation of robotic pollination performance in field experiments involves success rate of targeting, pollen consumption, pollination time, and fruit set rate. The amount of pollen consumed by a single flower is small, and every 60 flowers are used as the unit of measurement. The statistical summary of robotic pollination performance is presented in Table 2. Average success rates of targeting and fruit set rates in five different zones were 93.4% and 88.9%, respectively. The above two indicators are only 6.6% and 1.7% lower than hand pollination, but pollen consumption is reduced by 20% due to the characteristics of air–liquid spray and quantitative pollination.

15564967, 2025, 5, Downloaded from https://onlinelibrary.wiley.com/doi/10.1002/rob.22499 by Northwest Agri & Forestry, Wiley Online Library on [28/01/2026]. See the Terms and Conditions (https://onlinelibrary.wiley.com/terms-and-conditions) on Wiley Online Library for rules of use; OA articles are governed by the applicable Creative Commons License

TABLE 2 | Comparison of different pollination methods.

Pollination methods	Success rate of targeting (%)	Average pollen consumption of 60 flowers (g)	Average pollination time for a flower (s)	Fruit set rate (%)
Robotic pollination	93.4	0.20	1.2	88.9
Hand pollination	—	0.25	1.0	90.6
Electric sprayer	—	0.60	0.5	77.8



FIGURE 16 | Examples of grow-up kiwifruit that pollinated by the robot.

The multinozzle targeted pollination robot demonstrated several advantages compared with electric sprayer pollination, particularly in terms of pollen consumption and fruit set rate. The average pollen consumption of every 60 flowers was 0.20 g. And average pollination time for a single flower was 1.2 s. The pollen consumption of electrically powered spraying for pollination is 2 times higher in this study, yet the fruit set rate is lower by 11.1%. Indiscriminate pollination techniques (i.e., large-scale spraying and electric sprayer) for pollination result in pollen being sprayed onto nontarget areas, such as leaves and petals, which leads to pollen waste. It is noteworthy that the presence of strong winds could lead to the drifting of sprayed pollen droplets, serving as one of the primary factors for ineffective pollination. In the future, adding a wind deflector to the end-effector or applying electrostatic charges to the spray is a potential method to increase deposition (Grosshans 2023; Mehta et al. 2023).

A comparison was conducted between constructed multinozzle targeting pollination robot and prior research on kiwifruit robotics pollination. Gao et al. (2023) obtained an average pollination time of 2.0 s per kiwifruit flower with a single nozzle robot, which was 40% slower than this study. K. Li, Zhai et al. (2022) obtained a mean success rate of pollination of 89.59% with an average pollination time of 6 s per kiwifruit flower. Not only was the detection success rate 4.77% lower than in our study, but the pollination time was also 4 s longer than that of our robot. In the single-nozzle end-effector, the robotic arm pollinates only one flower at one time, while the multinozzle end-effector increases the number of flowers pollinated per motion, thus improving pollination efficiency.

A trade-off between fruit set rate and pollination time was required. Williams et al. (2021) designed a pollination system consisting of 42 nozzles that demonstrated the capability to target and pollinate 79.5% of flowers at a speed of 3.5 km/h, resulting in a fruit set rate of 71.6%. Despite achieving a higher average pollination rate, the fruit set rate was 16.9% lower than this paper. Although mobile targeting improves pollination efficiency, it reduces the success rate of targeting, causing some pollen to be sprayed outside the pistil area, resulting in pollen waste and a decrease in fruit setting rate. Because flowers grow in irregular patterns, each nozzle in the multinozzle end-effector cannot properly target the center of the flower's pistil while moving. Balancing the relationship between these factors requires further research in subsequent studies.

3.4 | Quality Evaluation of Kiwifruit Pollinated by Robot

Final fruits are important for assessing pollination effectiveness; kiwifruit quality was evaluated by size, weight, and seed number. Four months after pollination, in September 2023, fruit marked with tags (indicated the pollination methods and the number of the kiwifruit tree) were ripe for harvesting, as shown in Figure 16. Kiwifruit are sold by weight and size, making it an important measure of fruit quality. However, a variety of factors, including pollination, growing conditions, and vine health, influence fruit weight and size. Therefore, the control group was set closer to the experimental group to reduce the influence of external factors.

The box plots illustrate the impact of three pollination methods, that is, robotic pollination, hand pollination, and electric sprayer, on fruit quality. As shown in Figure 17a, the median of equatorial diameter for robotic pollination is 52.12 mm, which is 1.85 mm lower than that of hand pollination and 3.03 mm higher than that of electric sprayer. The data for robotic pollination exhibits some variability and includes several low outliers. Figure 17b presents the longitudinal diameter, where hand pollination results in the largest fruits, with a median around 71.04 mm, while the electric sprayer and robotic pollination have medians of roughly 72 and 70 mm, respectively. The longitudinal diameter distribution is more dispersed for the electric sprayer, while robotic pollination shows several low outliers. Figure 17c presents the fruit weight, showing similar patterns in median, quartiles, and data distribution as seen in the equatorial diameter.

The greater variability in the equatorial diameter, longitudinal diameter, and fruit weight for robotic pollination compared with hand pollination has three reasons. First, hand pollination adopts dry pollen, which remains active longer than that in

15564967, 2025, 5, Downloaded from https://onlinelibrary.wiley.com/doi/10.1002/rob.22499 by Northwest Agri & Forestry, Wiley Online Library on [28/01/2026]. See the Terms and Conditions (https://onlinelibrary.wiley.com/terms-and-conditions) on Wiley Online Library for rules of use; OA articles are governed by the applicable Creative Commons License

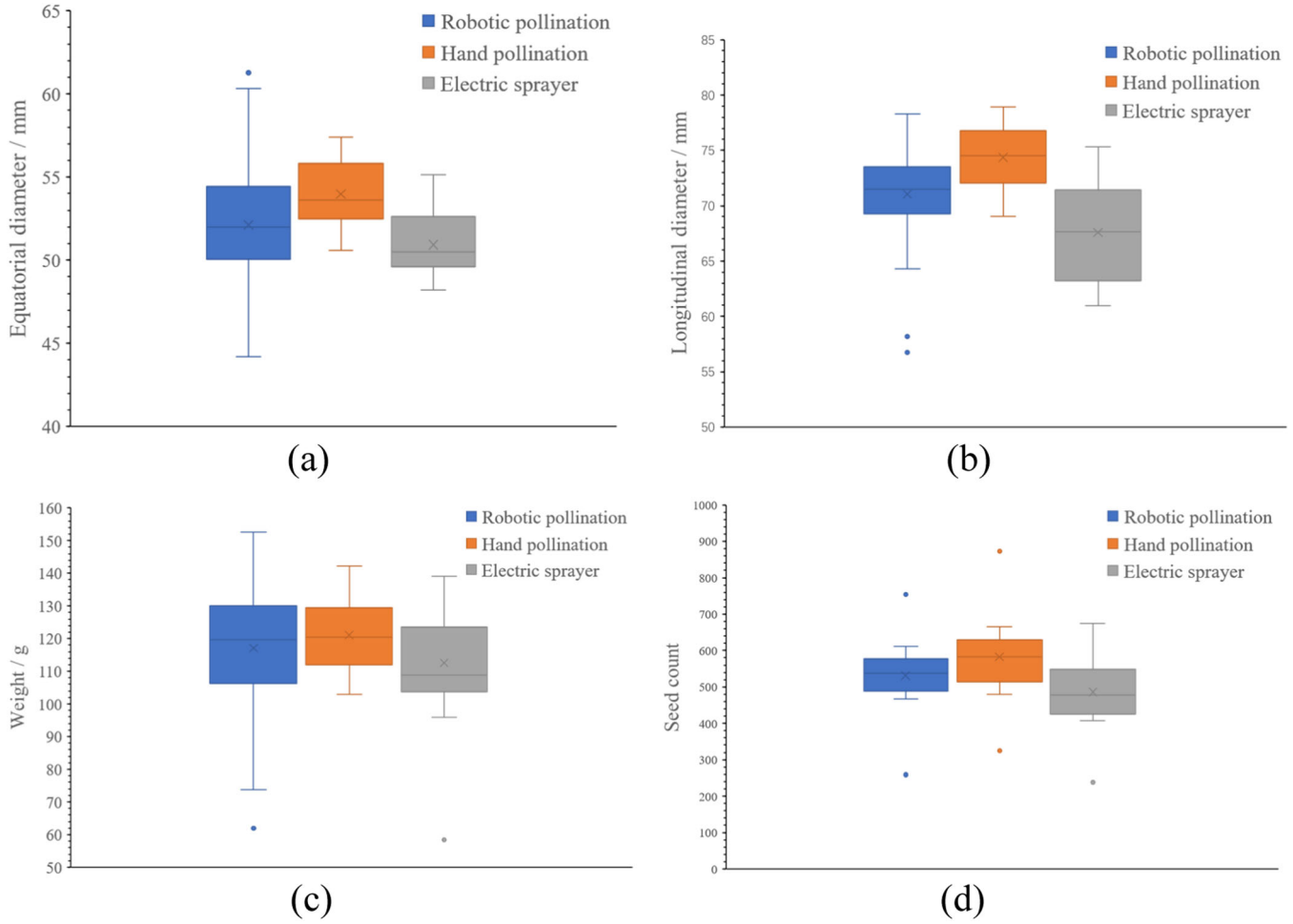


FIGURE 17 | Boxplot for quality evaluation of kiwifruit flower pollinated by a robot. (a) Equatorial diameter, (b) longitudinal diameter, (c) weight, and (d) seed count. Median is indicated with a horizontal line, boxes extend to the interquartile range, possible outliers are indicated with points.

pollen fluid. Second, the precision of hand pollination for the pistil area is higher than that of the multinozzle end-effector. Third, fruit thinning typically occurs in the control group about 1 month after pollination, aiming to eliminate small and malformed fruits and optimize vine resources for the cultivation of more desirable fruit. Although the preferential flower selection strategy adopted in this study means flower thinning, it cannot completely replace fruit thinning 1 month after pollination to ensure fruit set. The average seed count of robotic pollination is 531, which is 51 seeds per fruit lower than that of hand pollination as shown in Figure 17d. Hand pollination exhibits the least variability, whereas the seed count distribution for robotic pollination is more undispersed. The tighter distribution of seed count is due to the effectiveness of targeted pollination, ensuring successful pollen-pistil interaction.

In summary, hand pollination consistently performs best across all measured parameters with more concentrated data and fewer outliers. However, robotic pollination demonstrates substantial potential, achieving competitive results in terms of fruit size and weight. Despite its higher variability, robotic pollination offers a feasible and scalable alternative, especially with further technological refinements. The electric sprayer provides relatively average performance across all metrics. From the above results, the constructed pollination robot attained satisfactory performance. In the future, the pollination robot will add obstacle avoidance motion functions to enhance its autonomy (Bai et al. 2023; Tang et al. 2023). Besides, future research could explore optimizing robotic pollination technology to enhance its stability and effectiveness.

4 | Conclusions

In this research, a novel multinozzle kiwifruit pollination robot was developed for liberating human from heavy labor while mitigating pollen loss during the pollination of large orchards. Multinozzle end-effector was designed based on statistics of flower cluster size to raise efficiency. For this pollination robot, a strategy of preferential flowers selection and multinozzle targeting was designed and confirmed to achieve precise pollination. In field experiments, the success rate of targeting and fruit set rate was 93.4% and 88.9%, respectively, which showed the pollination robot can meet the requirements for kiwifruit precision pollination. Nevertheless, the influence of strong winds in open fields may result in the dispersion of sprayed pollen liquid droplets, potentially resulting in not only pollen waste but also inadequate pollination. Subsequent

15564967, 2025, 5, Downloaded from https://onlinelibrary.wiley.com/doi/10.1002/rob.22499 by Northwest Agri & Forestry, Wiley Online Library on [28/01/2026]. See the Terms and Conditions (https://onlinelibrary.wiley.com/terms-and-conditions) on Wiley Online Library for rules of use; OA articles are governed by the applicable Creative Commons License

enhancements for this pollination robot will focus on designing a device that induces a wind deflector and an electrostatic charge to enhance the adhesion capability of mist droplets, while concurrently exploring multiarm collaboration to enhance pollination velocity.

Acknowledgments

This work was partially supported by the National Natural Science Foundation of China (No. 32371999), Science and Technology Program of Xi'an City, China (No. 23NYGG0071), National Key Research and Development Program of China (No. 2022YFD1600700), Open Project of Key Laboratory of Agricultural Equipment for Hilly and Mountainous Areas in Southeastern China (Co-construction by Ministry and Province), Ministry of Agriculture and Rural Affairs, China (No. QSKF2023002), Central Public-interest Scientific Institution Basal Research Fund (No. 1610192023105), and National Foreign Expert Project, Ministry of Science and Technology, China (Nos. DL2022172003L and QN2022172006L).

Data Availability Statement

The data that support the findings of this study are available from the corresponding author upon reasonable request.

References

Bai, Y., B. Zhang, N. Xu, J. Zhou, J. Shi, and Z. Diao. 2023. "Vision-Based Navigation and Guidance for Agricultural Autonomous Vehicles and Robots: A Review." *Computers and Electronics in Agriculture* 205: 107584. https://doi.org/10.1016/j.compag.2022.107584.

Bhattarai, U., Q. Zhang, and M. Karkee. 2024. "Design, Integration, and Field Evaluation of a Robotic Blossom Thinning System for Tree Fruit Crops." *Journal of Field Robotics* 41: 1366–1385. https://doi.org/10.1002/rob.22330.

Broussard, M. A., M. Goodwin, H. M. McBrydie, L. J. Evans, and D. E. Pattemore. 2021. "Pollination Requirements of Kiwifruit (*Actinidia chinensis* Planch.) Differ Between Cultivars 'Hayward' and 'Zesy002'." *New Zealand Journal of Crop and Horticultural Science* 49, no. 1: 30–40. https://doi.org/10.1080/01140671.2020.1861032.

Castro, H., C. Siopa, V. Casais, et al. 2021. "Pollination as a Key Management Tool in Crop Production: Kiwifruit Orchards as a Study Case." *Scientia Horticulturae* 290: 110533. https://doi.org/10.1016/j.scienta.2021.110533.

Chen, S., X. Wang, and N. Cheng. 2021. "Ultrasound-Assisted Ethanol Extraction of *Actinidia arguta* Pollen Possesses Antioxidant Activity and Protects DNA From Oxidative Damage." *Journal of Food Biochemistry* 45: 13603. https://doi.org/10.1111/jfbc.13603.

Fan, M., J. Li, Y. Zhang, S. Qi, and Y. Tang. 2023. "Transforming Unmanned Pineapple Picking With Spatio-Temporal Convolutional Neural Networks." *Computers and Electronics in Agriculture* 214: 108298. https://doi.org/10.1016/j.compag.2023.108298.

Gao, C., L. He, W. Fang, et al. 2023. "A Novel Pollination Robot for Kiwifruit Flower Based on Preferential Flowers Selection and Precisely Target." *Computers and Electronics in Agriculture* 207: 107762. https://doi.org/10.1016/j.compag.2023.107762.

Gao, C., H. Jiang, X. Liu, et al. 2024. "Improved Binocular Localization of Kiwifruit in Orchard Based on Fruit and Calyx Detection Using YOLOv5x for Robotic Picking." *Computers and Electronics in Agriculture* 217: 108621. https://doi.org/10.1016/j.compag.2024.108621.

Gheshlaghi, E. A. 2019. "Effective Pollination Period and Its Influence on Fruit Characteristics of 'Hayward' Kiwifruit." *Advances in Horticultural Science* 33, no. 4: 537–542. https://doi.org/10.13128/ahsc-8186.

Gianni, T., and M. Vania. 2018. "Artificial Pollination in Kiwifruit and Olive Trees." In *Pollination in Plants*, edited by P. W. Mokwala, 59–80. https://doi.org/10.5772/intechopen.74831.

González, M. V., M. Coque, and M. Herrero. 1995. "Stigmatic Receptivity Limits the Effective Pollination Period in Kiwifruit." *Journal of the American Society for Horticultural Science* 120, no. 2: 199–202. https://doi.org/10.21273/jashs.120.2.199.

Grosshans, H. 2023. "Influence of Weak Electrostatic Charges and Secondary Flows on Pneumatic Powder Transport." *Canadian Journal of Chemical Engineering* 101, no. 5: 2347–2360. https://doi.org/10.1002/cjce.24824.

Hao, W., X. Ding, Z. He, et al. 2023. "Development and Evaluation of Precision Liquid Pollinator for Kiwifruit." *Computers and Electronics in Agriculture* 213: 108193. https://doi.org/10.1016/j.compag.2023.108193.

Jerram, E. M. 1979. "Pollination of Kiwifruit (*Actinidia chinensis* Planch.): Stigma-Style Structure and Pollen Tube Growth." *New Zealand Journal of Botany* 17, no. 3: 233–240. https://doi.org/10.1080/0028825X.1979.10426897.

Johnson, E. N., and J. G. Mooney. 2014. "A Comparison of Automatic Nap-of-the-Earth Guidance Strategies for Helicopters." *Journal of Field Robotics* 31, no. 4: 637–653. https://doi.org/10.1002/rob.21514.

Li, J., M. Broussard, N. Tomer, et al. 2022. "Honey Bee (*Apis Mellifera*) Hive Placement Is More Influential Than Orchard Layout on the Fruit Set of a Dioecious Crop." *Ecological Modelling* 472: 110074. https://doi.org/10.1016/j.ecolmodel.2022.110074.

Li, G., L. Fu, C. Gao, et al. 2022. "Multi-Class Detection of Kiwifruit Flower and Its Distribution Identification in Orchard Based on YOLOv5l and Euclidean Distance." *Computers and Electronics in Agriculture* 201: 107342. https://doi.org/10.1016/j.compag.2022.107342.

Li, K., W. Gong, Y. Shi, et al. 2023. "Predicting Positions and Orientations of Individual Kiwifruit Flowers and Clusters in Natural Environments." *Computers and Electronics in Agriculture* 211: 108039. https://doi.org/10.1016/j.compag.2023.108039.

Li, H., Z. Gu, D. He, et al. 2024. "A Lightweight Improved YOLOv5s Model and Its Deployment for Detecting Pitaya Fruits in Daytime and Nighttime Light-Supplement Environments." *Computers and Electronics in Agriculture* 220: 108914. https://doi.org/10.1016/j.compag.2024.108914.

Li, G., R. Suo, G. Zhao, et al. 2022. "Real-Time Detection of Kiwifruit Flower and Bud Simultaneously in Orchard Using YOLOv4 for Robotic Pollination." *Computers and Electronics in Agriculture* 193: 106641. https://doi.org/10.1016/j.compag.2021.106641.

Li, K., L. Zhai, H. Pan, Y. Shi, X. Ding, and Y. Cui. 2022. "Identification of the Operating Position and Orientation of a Robotic Kiwifruit Pollinator." *Biosystems Engineering* 222: 29–44. https://doi.org/10.1016/j.biosystemseng.2022.07.014.

Lippi, M., M. Santilli, R. F. Carpio, et al. 2023. "An Autonomous Spraying Robot Architecture for Sucker Management in Large-Scale Hazelnut Orchards." *Journal of Field Robotics* 41: 2114–2132. https://doi.org/10.1002/rob.22217.

Liu, X., X. Jing, H. Jiang, et al. 2024. "Performance Evaluation of Newly Released Cameras for Fruit Detection and Localization in Complex Kiwifruit Orchard Environments." *Journal of Field Robotics* 41, no. 4: 881–894. https://doi.org/10.1002/rob.22297.

Lohan, S. K., M. K. Narang, M. Javed, V. Kumar, A. Majumder, and P. Raghuvirsinh. 2022. "Optimization and Evaluation of Machine—Field Parameters of Remotely Controlled Two-Wheel Paddy Transplanter." *Journal of Field Robotics* 39, no. 6: 984–998. https://doi.org/10.1002/rob.22080.

McNeilage, M. A. 1991. "Gender Variation in *Actinidia deliciosa*, the Kiwifruit." *Sexual Plant Reproduction* 4: 267–273.

Mcpherson, H. G., A. C. Richardson, W. P. Snelgar, K. J. Patterson, and M. B. Currie. 2001. "Flower Quality and Fruit Size in Kiwifruit

15564967, 2025, 5, Downloaded from https://onlinelibrary.wiley.com/doi/10.1002/rob.22499 by Northwest Agri & Forestry, Wiley Online Library on [28/01/2026]. See the Terms and Conditions (https://onlinelibrary.wiley.com/terms-and-conditions) on Wiley Online Library for rules of use; OA articles are governed by the applicable Creative Commons License

(*Actinidia deliciosa*)." *New Zealand Journal of Crop and Horticultural Science* 29, no. 2: 93–101. https://doi.org/10.1080/01140671.2001.9514167.

Mehta, D., G. Sahu, M. K. Patel, et al. 2023. "Quality Evaluation of Tomatoes Coated by an Advanced Electrostatic Spray Coating System." *International Journal of Food Science & Technology* 58, no. 12: 6351–6361. https://doi.org/10.1111/ijfs.16743.

Meshram, A. T., A. V. Vanalkar, K. B. Kalambe, and A. M. Badar. 2022. "Pesticide Spraying Robot for Precision Agriculture: A Categorical Literature Review and Future Trends." *Journal of Field Robotics* 39, no. 2: 153–171. https://doi.org/10.1002/rob.22043.

Reji, M., and R. Kumar. 2022. "Response Surface Methodology (RSM): An Overview to Analyze Multivariate Data." *Indian Journal of Microbiology Research* 9, no. 4: 241–248. https://doi.org/10.18231/j.ijmr.2022.042.

Salinero, M. C., P. Vela, and M. J. Sainz. 2009. "Phenological Growth Stages of Kiwifruit (*Actinidia deliciosa* 'Hayward')." *Scientia Horticulturae* 121, no. 1: 27–31. https://doi.org/10.1016/j.scienta.2009.01.013.

Song, Y., S. Lee, J. Jo, et al. 2019. "Changes in Activity and Isozyme Patterns of Peroxidase and Chitinase in Kiwifruit Pollen." *Journal of Applied Botany and Food Quality* 92: 313–319. https://doi.org/10.5073/JABFQ.2019.092.042.

Tacconi, G., V. Michelotti, O. Cacioppo, and G. Vittone. 2016. "Kiwifruit Pollination: The Interaction Between Pollen Quality, Pollination Systems and Flowering Stage." *Journal of Berry Research* 6, no. 4: 417–426. https://doi.org/10.3233/JBR-160138.

Tang, Y., S. Qi, L. Zhu, X. Zhuo, Y. Zhang, and F. Meng. 2023. "Obstacle Avoidance Motion in Mobile Robotics." *Journal of System Simulation* 36, no. 1: 1–26. https://doi.org/10.16182/j.issn1004731x.joss.23-1297E.

Watson, M., and K. S. Gould. 1993. "The Development of Fruit Shape in Kiwifruit: Growth Characteristics and Positional Differences." *Horticultural Science and Biotechnology* 68, no. 2: 185–194. https://doi.org/10.1080/00221589.1993.11516342.

Williams, H., J. Bell, M. Nejati, et al. 2021. "Evaluating the Quality of Kiwifruit Pollinated With an Autonomous Robot." *Field Robotics* 1: 231–252.

Williams, H., M. Nejati, S. Hussein, et al. 2020. "Autonomous Pollination of Individual Kiwifruit Flowers: Toward a Robotic Kiwifruit Pollinator." *Journal of Field Robotics* 37, no. 2: 246–262. https://doi.org/10.1002/rob.21861.

Wu, S., J. Liu, X. Lei, et al. 2022. "Research Progress on Efficient Pollination Technology of Crops." *Agronomy* 12, no. 11: 2872. https://doi.org/10.3390/agronomy12112872.

Zhang, L., Y. Sui, X. Gao, and Z. Fu. 2005. "Structural Optimization Based on Response Surface Methodology." *Mechanics in Engineering* 27, no. 3: 35–39. https://doi.org/10.6052/1000-0992-2004-386.

15564967, 2025, 5, Downloaded from https://onlinelibrary.wiley.com/doi/10.1002/rob.22499 by Northwest Agri & Forestry, Wiley Online Library on [28/01/2026]. See the Terms and Conditions (https://onlinelibrary.wiley.com/terms-and-conditions) on Wiley Online Library for rules of use; OA articles are governed by the applicable Creative Commons License